



HAL
open science

Detectability of ultrahigh energy cosmic-ray signatures in gamma-rays

K. Kotera, D. Allard, M. Lemoine

► **To cite this version:**

K. Kotera, D. Allard, M. Lemoine. Detectability of ultrahigh energy cosmic-ray signatures in gamma-rays. *Astronomy and Astrophysics - A&A*, 2011, 527, 10.1051/0004-6361/201015259 . insu-03646048

HAL Id: insu-03646048

<https://insu.hal.science/insu-03646048>

Submitted on 21 Apr 2022

HAL is a multi-disciplinary open access archive for the deposit and dissemination of scientific research documents, whether they are published or not. The documents may come from teaching and research institutions in France or abroad, or from public or private research centers.

L'archive ouverte pluridisciplinaire **HAL**, est destinée au dépôt et à la diffusion de documents scientifiques de niveau recherche, publiés ou non, émanant des établissements d'enseignement et de recherche français ou étrangers, des laboratoires publics ou privés.

Detectability of ultrahigh energy cosmic-ray signatures in gamma-rays

K. Kotera^{1,2}, D. Allard³, and M. Lemoine¹

¹ Institut d'Astrophysique de Paris UMR7095 – CNRS, Université Pierre & Marie Curie, 98 bis boulevard Arago, 75014 Paris, France

² Department of Astronomy & Astrophysics, Enrico Fermi Institute, and Kavli Institute for Cosmological Physics, The University of Chicago, Chicago, Illinois 60637, USA
e-mail: kotera@uchicago.edu

³ Laboratoire Astroparticules et Cosmologie (APC), Université Paris 7/CNRS, 10 rue A. Domon et L. Duquet, 75205 Paris Cedex 13, France

Received 22 June 2010 / Accepted 11 November 2010

ABSTRACT

The injection of ultrahigh energy cosmic-rays in the intergalactic medium leads to the production of a GeV–TeV gamma-ray halo centered on the source location, through the production of a high electromagnetic component in the interactions of the primary particles with the radiation backgrounds. This paper examines the prospects for the detectability of such gamma-ray halos. We explore a broad range of astrophysical parameters, including the inhomogeneous distribution of magnetic fields in the large-scale structure, as well as various possible chemical compositions and injection spectra; and we consider the case of a source located outside clusters of galaxies. We demonstrate that the gamma-ray flux associated to synchrotron radiation of ultrahigh energy secondary pairs does not depend strongly on these parameters, and conclude that its magnitude ultimately depends on the energy injected into the primary cosmic-rays. We find that the gamma-ray halo produced by equal luminosity sources (with cosmic ray luminosity and source density chosen to reproduce the measured cosmic-ray spectrum) is far fainter than current or planned instrument sensitivities. Only rare and powerful steady sources, located at distances larger than several hundreds of Mpc and contributing to a fraction $\geq 10\%$ of the flux at 10^{19} eV might be detectable. We also discuss the gamma-ray halos that are produced by inverse Compton/pair production cascades seeded by ultrahigh energy cosmic-rays. This depends strongly on the configuration of the extragalactic magnetic fields; it is dominated by the synchrotron signal on a degree scale if the filling factor of magnetic fields with $B \gtrsim 10^{-14}$ G is smaller than a few percent. Finally, we briefly discuss the case of nearby potential sources such as Centaurus A.

Key words. astroparticle physics – gamma rays: general – magnetic fields

1. Introduction

The quest to identify the sources of ultrahigh energy cosmic-rays has long been associated with the search for their secondary radiative signatures. While propagating, the former indeed produce very high energy photons through their interactions with the ambient backgrounds; and gamma-rays should be valuable tools for identifying the birthplace of the primary cosmic-rays as they travel rectilinearly, in contrast to charged particles.

The detection of these high energy photon fluxes is however far from straightforward. On purely astrophysical grounds, the propagation of gamma rays with energies exceeding several TeV is obstructed by their relatively short pathlength of interaction with cosmic microwave background (CMB) and infrared photons. These interactions lead to the production of high energy electron and positron pairs which in turn up-scatter CMB or radio photons by inverse Compton processes, initiating electromagnetic cascades. One does not expect to observe gamma-rays of energy above ~ 100 TeV from sources located beyond a horizon of a few megaparsecs (Gould & Schröder 1967; Wdowczyk et al. 1972; Protheroe 1986; Protheroe & Stanev 1993). Below this energy, the detection of the gamma-ray signal originating from ultrahigh energy cosmic-rays depends on the luminosity and angular extension of the observed object and obviously on the sensitivity and angular resolution of the available instruments.

Intergalactic magnetic fields inevitably come into play because: i) primary cosmic-rays can be deflected by the magnetic field surrounding the source prior to the production of secondary photons/electrons/positrons; and ii) secondary electrons and positrons produced by cosmic-ray interactions or by photon-photon interactions can also be deflected by the intergalactic magnetic field during the cascade. In both cases, the ultimate gamma-ray emission can experience a sizable spread around the ultrahigh energy cosmic-ray source.

Aharonian (2002) and Gabici & Aharonian (2005) found that the magnetic field environment of the source may also lead to the generation of a multi-GeV gamma-ray halo around ultrahigh energy cosmic-ray sources. The idea is the following: for high enough energies and in the presence of a magnetic field large enough in the surroundings of the source, the electron and positron pairs produced through the interaction of ultrahigh energy particles with the ambient backgrounds may lose a significant fraction of their energy through synchrotron emission. This synchrotron component falls around ~ 10 GeV, below the pair creation threshold, hence it will not be affected by additional electromagnetic cascading. Assuming that the source is located at a distance of 100 Mpc, at the center of a homogeneously magnetized sphere of radius 20 Mpc with $B = 1$ nG, Gabici & Aharonian (2005) estimate that this signal would have an angular size of a fraction of degree (see also

Aharonian et al. 2010). It might therefore appear point-like to instruments such as the Fermi Space Telescope but as an extended source to future imaging Cerenkov telescopes.

This process is particularly interesting, because its signature could easily be differentiated from a point-like gamma-ray signal emitted by leptonic or hadronic channels inside the source, associated with the acceleration of particles to energies possibly well below 10^{19} eV. The dominant background to this synchrotron halo is actually the halo produced by multi-TeV electrons that undergo inverse Compton scattering on the cosmic microwave background and that are seeded by multi-TeV photons at $\gtrsim 100$ Mpc distance from the source (Aharonian et al. 1994). However, as discussed in the present paper, discrimination between these two signals should be possible thanks to the different dependences of the angular images on both physical parameters and energy. Then, one could argue that the detection of a synchrotron halo around a powerful source would constitute an unambiguous signature of acceleration to ultrahigh energies in this source: first of all, the inverse Compton cooling length of electrons of energy $1 \text{ TeV} \lesssim E_e \lesssim 10^{17}$ eV is smaller than 300 kpc, hence the gamma-ray signal of very high energy electrons produced in the source would appear point-like at distances $\gtrsim 100$ Mpc; furthermore, secondary electrons generally carry a few percent of the parent proton energy, so that $\gtrsim 10^{17}$ eV secondary electrons correspond to $\gtrsim 10^{19}$ eV protons; finally, if the radiating electrons are seeded away from the source by high energy nuclei, these nuclei must carry an energy $\gtrsim 10^{19}$ eV as lower energy nuclei are essentially immune to radiative losses.

Given our state of knowledge on the sources of ultrahigh energy cosmic rays, the detection of this halo would have a lasting impact on this field of research. The detectability of these signals thus deserves close scrutiny.

The production of gamma-ray signatures of ultrahigh energy cosmic-rays were studied numerically by Ferrigno et al. (2004) and Armengaud et al. (2006). However, the former authors focused their study on the Compton cascades following the production of ultrahigh energy photons and pairs close to the source and neglected the deflection imparted by the surrounding magnetic fields which dilutes the gamma-ray signal (Gabici & Aharonian 2005). In contrast, Armengaud et al. (2006) addressed both the synchrotron emission of secondary pairs and the Compton cascading down to TeV energies, albeit for the particular case of a source located in a magnetized cluster of galaxies. The high magnetic field that prevails in these environments increases the residence time of primary and secondary charged particles and thus also increases the gamma-ray flux.

The present paper aims to examine the prospects for the detectability of gamma-ray halos around ultrahigh energy cosmic-ray sources, relaxing most of the assumptions made in the above previous studies. In particular, we discuss the more general case of a source located in the field, outside clusters of galaxies. We focus our discussion on the synchrotron signal emitted by secondary pairs, which offers a possibility of unambiguous detection; nevertheless, the deflection and dilution of the Compton cascading gamma-ray signal at TeV energies is also discussed. Going further than Aharonian (2002) and Gabici & Aharonian (2005), we take into account the inhomogeneous distribution of the magnetic fields in the source environment. We also relax the assumption of a pure proton composition for ultrahigh energy cosmic-rays, which is implicit in the above studies. The chemical composition of ultrahigh energy cosmic-rays indeed remains an open question. While experiments such as the Fly's Eye and HiRes have suggested a transition from heavy to light above $\sim 10^{18.5}$ eV (Bird et al. 1993; Abbasi et al. 2005, 2010), the most

recent measurements made with the Pierre Auger Observatory point instead towards a heavy composition above 10^{19} eV (Unger et al. 2007; Abraham et al. 2009, 2010). As the energy losses and magnetic deflection of high energy nuclei differ from those of a proton of a same energy, one should naturally expect different gamma-ray signatures.

The layout of the present paper is as follows. In Sect. 2, we first test the dependence of the gamma-ray flux produced by ultrahigh energy cosmic-rays on the type, intensity, and structure of magnetized environments. We also discuss the effects of various chemical compositions and injection spectra. We draw conclusions about the robustness of the gamma-ray signature according to these parameters and find that the normalization and thus the detectability of this flux ultimately depends on the energy injected into the primary cosmic-rays. In Sect. 3, we discuss the detectability of ultrahigh energy cosmic-ray signatures in gamma rays. Applying the results of our calculations, we show that the average type of sources contributing to the ultrahigh energy cosmic ray spectrum produces a gamma-ray flux more than two orders of magnitudes lower than the sensitivity of the current and upcoming instruments. We then explore the case of rare powerful sources of cosmic-ray luminosity higher than an energy 10^{19} eV of $L_{19} \gtrsim 10^{44-46} \text{ erg s}^{-1}$. We assume throughout this paper that sources emit isotropically and discuss how our conclusions are modified for beamed emission in Section 4. The gamma-ray signatures of those sources could be detectable provided that they are located far enough away not to overshoot the observed cosmic-ray spectrum. Finally, we also briefly discuss the detection of nearby sources, considering the radiogalaxy Centaurus A as a prototypical example. We draw our conclusions in Sect. 4.

2. Simulations

As mentioned above, we focus our discussion on the synchrotron signal that can be produced close to the source by very high energy electrons and positrons, which are produced themselves by the interactions of primary cosmic-rays. The signal associated with inverse Compton cascades of these electrons/positrons on radiation backgrounds is discussed in Sect. 3.3.

The secondary electrons and positrons are created through one of the three following channels: i) by the decay of a charged pion produced during a photo-hadronic interaction ($A \gamma \rightarrow \pi^+ + \dots$, then $\pi^+ \rightarrow \mu^+ \nu_\mu$, and $\mu^+ \rightarrow e^+ \nu_e \bar{\nu}_\mu$, with A a cosmic ray nucleus); ii) by photo pair-production during an interaction with a background photon ($A \gamma \rightarrow e^+ e^- + \dots$); or iii) by the disintegration of a neutral pion into ultrahigh energy photons, which then interact with CMB and radio backgrounds to produce electron and positron pairs ($A \gamma \rightarrow \pi^0 + \dots$, then $\pi^0 \rightarrow 2\gamma$, and $\gamma \gamma_{\text{bg}} \rightarrow e^+ e^-$, with γ_{bg} a cosmic background photon). In all cases, the resulting electrons and positrons typically carry up to a few percent of the initial cosmic-ray energy.

While propagating in the intergalactic medium, these ultrahigh energy electrons and positrons up-scatter CMB or radio photons through inverse Compton processes and/or they lose energy through synchrotron radiation. Following Gabici & Aharonian (2005), the effective inverse Compton cooling length¹ on the CMB and radio backgrounds can be written as

¹ We recall that at very high energy, pair production ($\gamma \gamma_{\text{bg}} \rightarrow e^+ e^-$) transfers energy to one of the pairs. The inverse Compton scattering of photons ($e \gamma_{\text{bg}} \rightarrow e \gamma$) occurring in the Klein-Nishina regime, nearly all the electron or positron energy is again transferred to the up-scattered photon. Thus, the initial electron energy in a cascade is degraded very

$x_{e\gamma} \approx 5 \text{ Mpc} (E_e/10^{18} \text{ eV})^{\alpha_{IC}}$, with $\alpha_{IC} = 1$ if the electron energy $E_e \lesssim 10^{18} \text{ eV}$ and $\alpha_{IC} \approx 0.25$ if $10^{18} \text{ eV} \lesssim E_e \lesssim 10^{20} \text{ eV}$. Above 10^{18} eV , the scaling of the cooling length actually depends on the assumptions made for the radio background, which are unfortunately not very well constrained. The possible differences that such uncertainties could introduce should however not affect the results discussed in this paper. This length scale has to be compared with the synchrotron cooling length

$$x_{eB} \sim 3.8 \text{ kpc} \left(\frac{B}{10 \text{ nG}} \right)^{-2} \left(\frac{E_e}{10^{19} \text{ eV}} \right)^{-1}, \quad (1)$$

where B is the magnetic field intensity (assumed to be homogeneous over this distance) and E_e the electron or positron energy.

As discussed in Gabici & Aharonian (2005), the opposite scalings of $x_{e\gamma}$ and x_{eB} with electron energy imply the existence of a cross-over energy E_\times , which depends on B and is such that beyond E_\times , electrons mainly cool via synchrotron instead of undergoing an inverse Compton cascade. For a magnetic field of intensity $B = 10^{-9} B_{\text{nG}} \text{ G}$, we find that $E_\times \sim 10^{18} \text{ eV} B_{\text{nG}}^{-1}$ for $B_{\text{nG}} \gtrsim 1$, $E_\times \sim 10^{18} \text{ eV} B_{\text{nG}}^{-1.6}$ for $1 \gtrsim B_{\text{nG}} \gtrsim 0.1$, and $E_\times \sim 10^{20} \text{ eV} B_{\text{nG}}^{-1}$ for $0.1 \gtrsim B_{\text{nG}}$ (see Fig. 1 of Gabici & Aharonian 2005; and see Lee 1998, for further details about the cascade physics).

Finally, the emitted synchrotron photon spectrum peaks at the energy:

$$E_{\gamma,\text{syn}} \sim 68 \text{ GeV} \left(\frac{B}{10 \text{ nG}} \right) \left(\frac{E_e}{10^{19} \text{ eV}} \right)^2. \quad (2)$$

2.1. Magnetic field configuration

Our current knowledge of the structure of magnetic fields at large scales is very poor. It mainly stems from the lack of observations due to the intrinsic weakness of the fields. Moreover, no satisfactory theory has been established to explain the origins of these fields and the subsequent magnetic enrichment of the Universe. For more than a decade, numerical simulations have endeavored to model the distribution of the magnetic field on large scales. One may cite in particular the works of Ryu et al. (1998), Dolag et al. (2004, 2005), Sigl et al. (2004), and Das et al. (2008). In these studies, magnetized seeds are injected into a cosmological simulation and the overall magnetic field then evolves coupled with the underlying baryonic matter. The final amplitude of the field is set to adjust the measured intensity inside clusters of galaxies (in Das et al. 2008, the amplitude is not arbitrary but is directly estimated from the gas kinetic property and corresponds nevertheless to the observations inside clusters). Unfortunately, these various simulations do not converge on the present-day configuration of extragalactic magnetic fields (see for example Fig. 1 of Kotera & Lemoine 2008a) and consequently, they diverge as to the effect of these magnetic fields on the transport of ultrahigh energy cosmic-rays. The cause of this difference likely lies in the choice of initial data, which cannot be constrained with our current knowledge. Given that these simulations are time consuming, these tools cannot be considered as practical.

In view of this situation, we explore the influence of three typical types of magnetic field structures on the gamma-ray

slowly, until the electron or positron energy is either radiated in synchrotron, or the photon energy falls beneath the pair production threshold. For this reason, one may consider the cascade ($e \rightarrow \gamma \rightarrow e\dots$) as the disintegration of one single particle, which loses energy over an effective loss length $x_{e\gamma}$ (Stecker 1973; Gould & Rephaeli 1978).

emission, following the method developed by Kotera & Lemoine (2008a). We map the magnetic field intensity distribution according to the underlying matter density ρ , assuming the relation $B = B_0 f(\rho)$, where B_0 is a normalization factor, and the dimensionless function f may be modelled as

$$f_{\text{iso}}(\rho) = \rho^{2/3}, \quad (3)$$

$$f_{\text{ani}}(\rho) = \rho^{0.9}, \quad (4)$$

$$f_{\text{contrast}}(\rho) = \rho \left[1 + \left(\frac{\rho}{\langle \rho \rangle} \right)^{-2} \right]^{-1}. \quad (5)$$

We note that B_0 corresponds approximately to the mean value of the magnetic field in the Universe. These phenomenological relationships greatly simplify the numerical procedure for obtaining a map of the extragalactic magnetic field since a pure dark matter (i.e. non hydrodynamical) simulation of large-scale structure provides a sufficiently good description of the density field. These relationships are motivated by physical arguments related to the mechanism of amplification of magnetic fields during structure formation and encapture the scalings observed in numerical simulations to within the uncertainty inherent in these simulations (see the corresponding discussion in Dolag 2006; and Kotera & Lemoine 2008a). The first relation is typically expected if baryonic matter undergoes an isotropic collapse. In dense regions of the Universe where viscosity and shear effects govern the evolution of the magnetized plasma however, the relation would get closer to Eq. (4). This formula can be derived analytically in the case of an anisotropic collapse along one or two dimensions, in for example filaments or sheets (King & Coles 2006). The last model is an ad-hoc modeling of the suppression of magnetic fields in the voids of large structure that leaves unchanged the distribution in the dense intergalactic medium (meaning $\rho > \langle \rho \rangle$). It thus allows us to model a situation in which the magnetic enrichment of the intergalactic medium is related to structure formation, for instance by means of the pollution by starburst galaxies and/or radiogalaxies (see the corresponding discussion in Kotera & Lemoine 2008b). In the following, we will refer to these three models as ‘‘isotropic’’, ‘‘anisotropic’’ and ‘‘contrasted’’ respectively.

To form a representative sample of the underlying matter density on large scales, we use a three-dimensional output (at redshift $z = 0$) of a cosmological dark matter simulation provided by Colombi. It assumes a Λ CDM model with $\Omega_m = 0.3$, $\Omega_\Lambda = 0.7$ and Hubble constant $h \equiv H_0/(100 \text{ km s}^{-1} \text{ Mpc}^{-1}) = 0.7$. The simulation models a $200 h^{-1} \text{ Mpc}$ comoving periodic cube divided into 256^3 cells, where the dark matter overdensity is computed. We do not resolve structures below the Jeans length, which implies that we can identify the computed Dark Matter distribution with a gas distribution.

2.2. Numerical code

We compute the gamma-ray signal with numerical Monte Carlo simulations, using the code presented in Kotera et al. (2009). In a first step, we propagate ultrahigh energy cosmic-rays (protons and heavier nuclei) in one of the three-dimensional magnetic field models described above. The coherence length λ_B of the magnetic field is assumed to be constant throughout space and is set to 100 kpc. This certainly is somewhat ad-hoc but the coherence scale enters the calculation of the deflection angle in the form $B \sqrt{\lambda_B}$, hence discussing various normalizations of the magnetic field strength, as we do further below, allows us to encapture different possible values for λ_B . Furthermore, 100 kpc seems a reasonable compromise between an upper limit

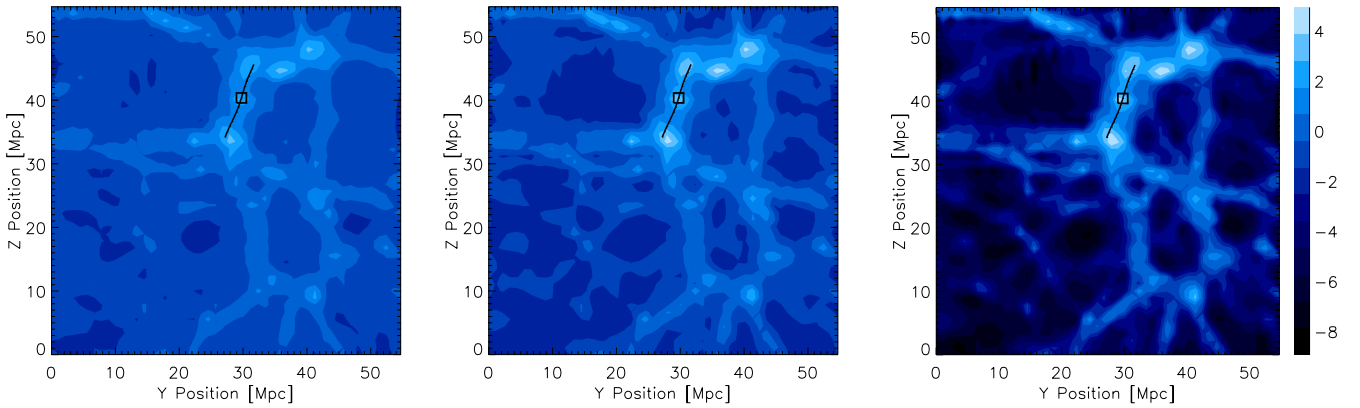


Fig. 1. Distribution of the magnetic field intensity in the region surrounding an ultrahigh energy cosmic-ray source. Each panel is a 1.1 Mpc thick (size of a grid cell) slice of the simulated Universe, cut along the axis perpendicular to the observed plan. *From left to right*, the distribution is “isotropic” (Eq. (3)), “anisotropic” (Eq. (4)), and “contrasted” (Eq. (5)). The color code is the same for all the panels and the values indicated on the right hand side correspond to the logarithm of the magnetic field intensity in nano-gauss. The black line indicates the axis of the filament that is studied throughout this paper and the black square the chosen position of the source. The normalization factor equals $B_0 = 1$ nG.

of a few hundreds of kpc for λ_B based on the turnaround time of the largest eddies (Waxman & Bahcall 1999) and typical galactic scales $\sim 10\text{--}30$ kpc (see Kotera & Lemoine 2008a, for a detailed discussion). The generation of secondary photons and electrons and positrons through pion production is treated in a discrete manner, as in Allard et al. (2006) for nuclei projectiles with $A > 1$ and with SOPHIA (Mücke et al. 1999) for proton and neutron cosmic-rays. Electron and positron pair creation through photo-hadronic processes is implemented as in Armengaud et al. (2006). For each time step (chosen to be much larger than the typical mean free path of pair photo-production processes), we assume that an ensemble of electron and positron pairs are generated with energies distributed according to a power law, and maximum energy depending on the primary particle. The use of an improved pair spectrum as computed in Kelner & Aharonian (2008) would lower the gamma-ray flux resulting from direct pair production by a factor of a few in the range $E_\gamma \lesssim 10$ GeV, and leave unchanged the prediction at a higher energy (Armengaud, priv. comm.). Furthermore, we show in the following that direct pair-production processes provide a subdominant contribution to the overall gamma-ray flux in the range $E_\gamma \gtrsim 0.1$ GeV, hence the overall difference is expected to be even smaller.

We investigate in this paper the possible detection of photons in the GeV–TeV energy range. Equation (2) suggests that, unless the source is embedded in a particularly strong field, the major contribution in this range will come from electrons of energy $E_e \gtrsim 10^{18}$ eV. The flux will thus essentially result from cosmic-rays of energy higher than $E \sim 10^{19}$ eV. For this reason, we chose to inject cosmic-rays at the source between $E_{\min} = 10^{17}$ eV and $E_{\max} = 10^{20.5}$ eV. We assume our source to be stationary with (isotropic) cosmic-ray luminosity integrated over $E = 10^{19}$ eV of $L_{E,19} = 10^{42\text{--}46}$ erg s^{-1} , and a spectral index of $\alpha = 2.3$.

We take into account photo-hadronic interactions with CMB and infrared photons. The diffuse infrared background is modelled according to the studies of Stecker et al. (2006). We do not take into account redshift evolution, as its effect is negligible compared to the uncertainties in our other parameters. We also neglect baryonic interactions in view of the negligible density in the source environment.

Once the secondary particles produced during the propagation have been computed, we calculate the synchrotron photon fluxes, taking into account the competition with inverse Compton scattering by performing Monte Carlo simulations over steps of size 100 kpc. The mean effective electron loss length is calculated following Gabici & Aharonian (2005), using the radio background data of Clark et al. (1970). We assume that each electron emits a synchrotron photon spectrum $dN_\gamma/dE_\gamma \propto E_\gamma^{-2/3}$ with a sharp cut-off above $E_c \sim (2/3) E_{\gamma,\text{syn}}$, where $E_{\gamma,\text{syn}}$ is given by Eq. (2).

For the photons produced through the neutral pion channel, we draw the interaction positions with CMB and radio photons using the mean free paths computed by Lee (1998). We assume that one of the electron-positron pair inherits the total energy of the parent photon.

2.3. Synchrotron signal for various magnetic field configurations

We first study the influence of inhomogeneous magnetic fields on the gamma-ray flux produced by ultrahigh energy cosmic-rays near their source. In particular, we examine the case of a source placed in a rather dense region of a filament of large-scale structure (see Fig. 1). On the transverse scale of the structure l_\perp , of the order of a few Mpc, one expects the secondary electrons and positrons to be distributed isotropically around the source. A population of ultrahigh energy cosmic-rays seeds the intergalactic medium with secondary pairs in a roughly homogeneous manner on the energy-loss length scale of the interaction process λ , i.e., the number of electrons/positrons injected per unit time per unit distance to the source $dN_e/dr dt$ does not depend on r as long as $r \ll \lambda$. For ultrahigh energy protons, this length scale is ~ 1 Gpc above 10^{19} eV for pair production and ~ 100 Mpc above 10^{20} eV for pion production. From the point of view of secondary synchrotron γ emission, however, the emission region is limited to the fraction of space in which the magnetic field is sufficiently intense for synchrotron cooling to predominate over inverse Compton cooling.

Most gamma-rays are produced by electrons of energy $E_e \gtrsim 10^{19}$ eV, themselves produced through pion production by protons of $E_p \gtrsim 10^{20}$ eV. In the absence of significant deflection

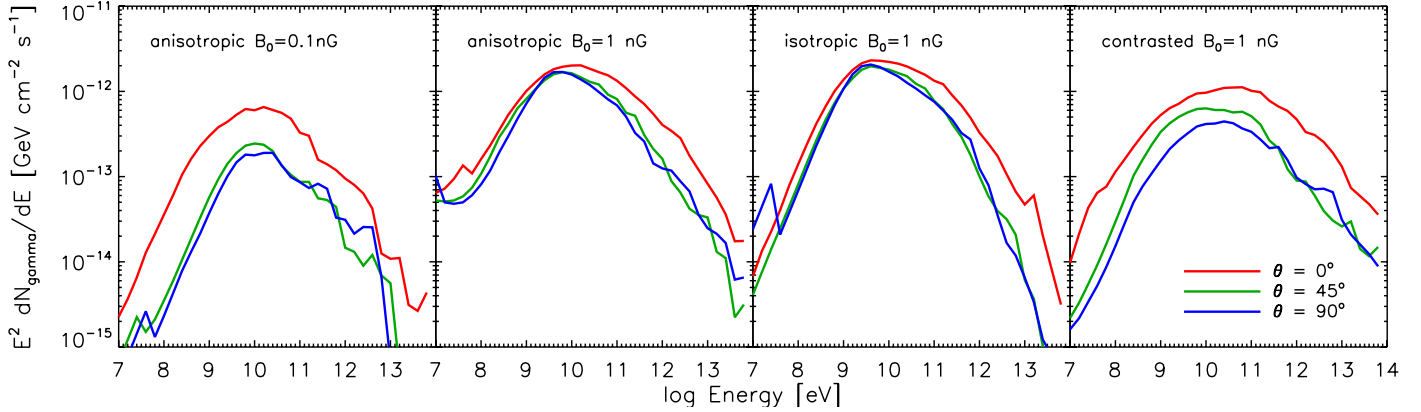


Fig. 2. Flux of photons produced by synchrotron emission for a filament observed from the directions forming the indicated angles with its axis. The filament is located at 100 Mpc and harbors a source that injects a pure proton composition with (isotropic) luminosity of $L_{E,19} = 10^{42}$ erg/s and a spectral index of 2.3. The four panels represent various models of magnetic fields. *From left to right*: “anisotropic” with $B_0 = 0.1$ nG, “anisotropic” with $B_0 = 1$ nG, “isotropic” with $B_0 = 1$ nG, and “contrasted” with $B_0 = 1$ nG.

experienced by these primary particles, one expects the synchrotron emission to be enhanced along the filament axis, where the magnetic field maintains a high value over a longer length than along the perpendicular direction (see Fig. 1). The whole structure where $x_{eB} < x_{e\gamma}$, i.e. $B_{\text{IGM}} \gtrsim 0.5 \text{ nG} (E_e/10^{19} \text{ eV})^{-3/4}$ is then illuminated by synchrotron radiation from electrons and positrons provided that $x_{eB} < ct_{\text{esc}}$, where t_{esc} denotes the escape timescale from the magnetized region. For a magnetic field with $B \sim 10 \text{ nG}$ and coherence length $\lambda_B \lesssim 100 \text{ kpc}$, the Larmor time $t_L \sim 1 \text{ Mpc} (E_e/10^{19} \text{ eV})(B/10 \text{ nG})^{-1} \sim \lambda_B$, hence confinement is marginal and the escape length $t_{\text{esc}} \sim l_{\perp} \gg x_{eB}$ (see Casse et al. 2002, for more details on the escape length).

At a given energy E_e , the ratio of the fluxes along to those perpendicular to the filament should be of the order of a/b , where a and b are the characteristic lengths of the axis of the filament where $B_{\text{IGM}} \gtrsim 0.5 \text{ nG} E_e^{-3/4}$.

Figure 2 indeed depicts this effect. It represents the synchrotron emission produced by a filament at a distance of 100 Mpc, embedding a source of luminosity $L_{E,19} = 10^{42} \text{ erg s}^{-1}$ and an injection spectral index of 2.3. One can see that the highest and lowest flux values differ by of a factor of ~ 2 – 5 , which corresponds to the ratio of the filament major to minor axis. For a narrower or longer filament, this interval would be more pronounced – which does not necessarily mean that the flux would be enhanced along the filament axis.

This difference in flux according to the observation angle disappears at low energy for the second and third panels of Fig. 2. This is related to the combined effect of the magnetic field configuration and the fraction of electrons producing the observed peak of gamma-rays. It corresponds to a coincidence and should not be viewed as an effect of the diffusion of primary protons. We indeed tested that these differences remain when cosmic-rays are forced to propagate rectilinearly. For the “contrasted” magnetic field, the gamma-ray fluxes are overall lower, as the field strength diminishes sharply outside the central part of the filament. The orthogonal section of the filament is thus substantially magnetized only over a short length, which consequently reduces the gamma-ray flux observed from 90° . For the isotropic and anisotropic cases with $B_0 = 1$ nG, electrons and positrons experience a weaker field on average when they cross the filament orthogonally, instead of traveling through their entire length. For the flux observed at 90° , photons with energy < 10 GeV are thus generated by electrons of slightly higher energy (E_{90}) than in the

0° case (E_0). By coincidence, E_{90} corresponds approximately to the peak of distribution of secondary electrons, whereas E_0 is shifted according to the peak. The flux observed at 90° is thus amplified for energies < 10 GeV because of the enhanced number of electrons contributing to the emission, which reduces the differences in fluxes at various observation angles. Finally, for the anisotropic case with $B_0 = 0.1$ nG, the emission is suppressed when the filament is not observed along its major axis, because of the weak mean field that particles experience (the mean field remains reasonably strong along the axis). The gap between the flux at 0° and the other cases stems from this effect.

Most of all, Fig. 2 demonstrates that the photon flux around $E_\gamma \sim 10$ GeV is fairly robust with respect to the various magnetic field configurations, which can be understood from Fig. 1: the extent of the magnetized region above $B \sim 1$ nG is indeed not fundamentally modified by the chosen distribution and the photon flux is hardly more sensitive to the overall intensity of the field (in particular, we tested that a value of $B_0 = 10$ nG does not affect the results of more than a factor of 2, for all magnetic configurations). All in all, for a quite reasonable normalization of the magnetic field, meaning an average $B_0 \sim 0.1$ – 10 nG at density contrasts of unity, and for various scalings of the magnetic field with density profile, the variations in flux remain smaller than an order of magnitude in the range $E_\gamma \sim 10$ – 1000 GeV.

Figure 2 also illustrates that the energy at which the signal peaks depends only weakly on the normalization of the magnetic field B_0 , and this remains true up to a few nano-gauss. This can be understood qualitatively, assuming for simplicity the field to be homogeneous over the area of interest, with strength B_0 . For $B_0 = 1$ nG, the electron cross-over energy E_\times beyond which electrons radiate in synchrotron is $E_\times \simeq 10^{18} \text{ eV}$ (see the discussion in Sect. 2). However, the energy spectrum $E_e dN_e/dE_e$ of secondary electrons deposited in the source vicinity peaks at $\sim 10^{19} \text{ eV}$, as a result of the competition between the opposite scalings with energy of the abundance of parent protons and the parent proton energy-loss rate. Therefore, the synchrotron signal is expected to peak at $E_\gamma \sim 10$ GeV (see Eq. (2) with $B_0 = 1$ nG and $E_e = 10^{19} \text{ eV}$). For $B_0 = 0.1$ nG, the cross-over energy $E_\times \simeq 4 \times 10^{19} \text{ eV}$, so that one should use $E_e = 4 \times 10^{19} \text{ eV}$ in Eq. (2) with $B_0 = 0.1$ nG, giving $E_\gamma \sim 10$ GeV again: the higher typical electron energy (among those radiating in synchrotron) compensates for the lower value of B_0 . As B_0 is increased significantly above 1 nG, the peak location of the gamma-ray

signal will increase in proportion, as most of the secondary electron flux can be radiated in synchrotron.

The flux should be cut off above $E_\gamma \sim 10$ TeV because of the opacity of the Universe to photons above this energy. This effect is not represented in these plots for simplicity, as its precise spectral shape depends on the distance d to the source (while the sub-TeV gamma-ray flux scales in proportion to L_{cr}/d^2).

At lower energy ($E_\gamma \lesssim 1$ GeV), the flux intensity can vary by more than two orders of magnitude depending on the chosen magnetic configuration. In the low energy range, magnetic confinement indeed starts to play an important role. Furthermore, the inverse Compton energy-loss length shortens drastically at these energies, so that only strong magnetic fields can help avoiding the formation of an electromagnetic cascade and lead instead to synchrotron emission in the filament.

2.4. Synchrotron signal for various chemical compositions and injection spectra

In this section, we discuss the effect of the injected chemical composition and the spectral index at the source. As discussed above, there are conflicting claims as to the measured chemical composition at ultrahigh energies; in particular, the HiRes experiment reports a light composition (Abbasi et al. 2010), while the Pierre Auger Observatory measurements point toward a composition that becomes increasingly heavier at energies above the ankle (Abraham et al. 2010). Theory is here of little help, as the source of ultrahigh energy cosmic-rays is unknown; protons are usually considered as prime candidates because of their large cosmic abundance, but at the same time one may argue that a large atomic number facilitates acceleration to high energy.

In this framework, Lemoine & Waxman (2009) proposed to test the chemical composition of ultrahigh energy cosmic-rays on the sky, using the anisotropy patterns measured at various energies, instead of relying on measurements of the depth of maximum shower development. It is shown in particular that, at equal magnetic rigidities E/Z , one should observe a comparable or stronger anisotropy signal from the proton component than from the heavy nuclei component emitted by the source, even if the source injects protons and heavy nuclei in equal numbers at a given energy. When compared to the 99% c.l. anisotropy signal reported by the Pierre Auger Observatory at energies above 5.7×10^{19} eV (Abraham et al. 2007, 2008a), one concludes that: if the composition is heavy at these energies, and if the source injects protons in at least equal numbers (at a given energy) as heavy nuclei, then one should observe a comparable or stronger anisotropy pattern above $5.7 \times 10^{19}/Z$ eV.

Future data will hopefully cast light on this issue, but in the meantime it is necessary to consider a large set of possible chemical compositions. We thus consider the following injection spectra:

1. two pure proton compositions with indices $\alpha = 2.3$ and 2.7 . A soft spectral index of ~ 2.7 seems to be favored to fit the observed cosmic-ray spectrum in the case of a pure proton composition, especially in the “dip-model” proposed by Berezhinsky et al. (2006), where the transition between the Galactic and extragalactic components occurs at relatively low energy ($E \sim 10^{17.5}$ eV);
2. a proton-dominated mixed composition with spectral index $\alpha = 2.3$, based on Galactic cosmic-ray abundances as in Allard et al. (2006). This spectrum is mostly proton dominated at ultrahigh energies;
3. a pure iron composition with spectral index $\alpha = 2.3$;

4. a mixed composition that was proposed by Allard et al. (2008), which consists 30% of iron. In this injection, the maximum proton energy is $E_{\text{max,p}} = 10^{19}$ eV (Allard et al. 2008, considered $E_{\text{max,p}} = 4 \times 10^{19}$ eV but an equally satisfying fit to the spectrum can be obtained for a lower value). Assuming that heavy elements are accelerated to an energy $Z \times E_{\text{max,p}}$, and because of the propagation effects that disintegrate intermediate nuclei preferentially compared to heavier nuclei, one would then measure on the Earth a heavy composition at the highest energy. The resulting detected spectrum allows us to reproduce the maximum depth of shower measurements of the Pierre Auger Observatory. However, the anisotropy pattern should also appear in this case at energies of the order of a few EeV, as discussed above. An injection spectrum of 2.0 is necessary to fit the observed cosmic-ray spectrum.

For the first three cases, the maximum proton injection energy is $E_{\text{max,p}} = 10^{20.5}$ eV. In all cases, we assume $E_{\text{max,Z}} = Z \times E_{\text{max,p}}$ for a nucleus of charge number Z (an exponential cut-off is assumed).

Figure 3 presents the fluxes obtained for these different injection spectra. The source is again located in the filament described earlier, at a distance of 100 Mpc, and has a luminosity above $E = 10^{19}$ eV of $L_{E,19} = 10^{42}$ erg s^{-1} . Owing to the comparatively larger number of protons at low energy, the photon flux below 1 GeV is amplified in the case of an injection spectrum of 2.7 compared to a 2.3 index. For similar reasons, the flux at higher energies (≥ 10 GeV) is lower.

The shift in amplitude between the fluxes produced by the different compositions can be understood as follows. The energy of the electrons and positrons produced by photo-disintegration is proportional to the nucleus Lorentz factor $E_e \propto \Gamma_A \propto E_A/A$. Hence at a given electron energy, the amount of injected energy by heavy nuclei is reduced if the spectral index is ≥ 2 . In addition, pion production via baryonic resonance processes on the CMB photons occur at energies higher than for protons ($E \gtrsim 10^{20}$ eV). The flux produced by the mixed “Galactic” composition with a 2.3 injection obviously differs only slightly from that produced by protons with the same spectral index as this composition is dominated by protons.

The above trends can also be noted in Fig. 4, which reveals a smaller contribution of photo-disintegration processes (in black dotted and pale blue dash-dotted lines) than for a proton composition. The yield of the electrons and positrons produced by photo-pair production (in blue dashed lines) is not as strongly attenuated, however, because the secondary nucleons are emitted above the pair production threshold (but below the pion photo-production threshold). The second bump at lower energy in the neutral pion channel (pale blue dash-dotted line) is related to the production of photons via the giant dipole resonance process.

Finally, the flux is suppressed for an iron-enriched mix composition, because of the relatively low cut-off energy, $E_{\text{max,p}} = 10^{19}$ eV. In this case, $E_{\text{max,p}}$ is lower than the pion production threshold energy for protons, and the heavy nuclei maximum energy is also lower than the pion production threshold, so this channel of secondary e^+e^- injection disappears.

3. Discussion on detectability

3.1. Synchrotron signal from equal luminosity sources

Our study indicates that around ~ 10 – 100 GeV, the gamma-ray flux produced by the propagation of ultrahigh energy

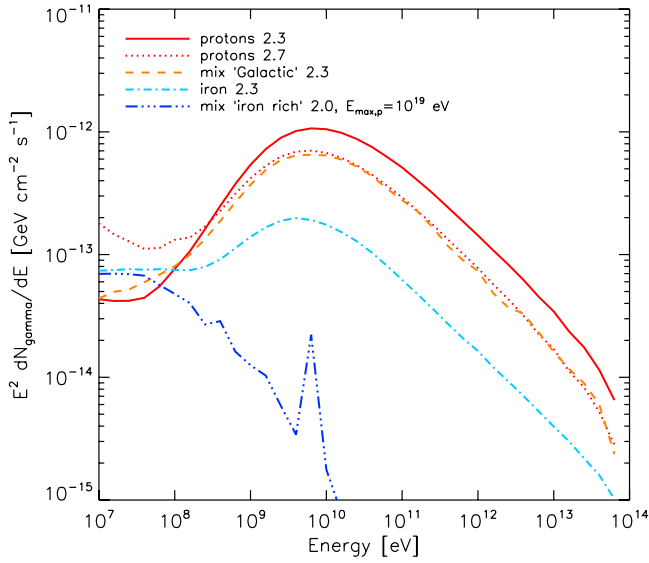


Fig. 3. Photon flux produced by synchrotron emission for different source injections. We chose an “anisotropic” distribution of the magnetic field with normalization $B_0 = 1$ nG. The source has a luminosity of $L_{E,19} = 10^{42}$ erg s^{-1} , and is located in the filament described previously, at a distance of 100 Mpc. The average flux integrated over all angular lines of sight are presented.

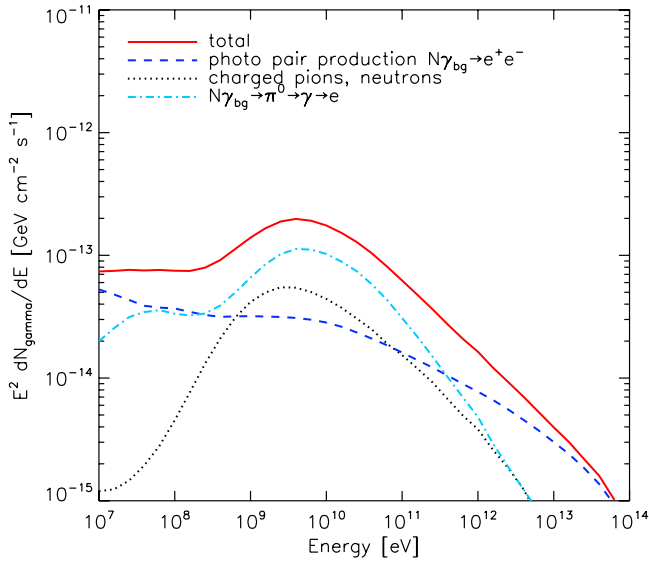


Fig. 4. Same as Fig. 3, but for the particular case of a pure iron injection with spectral index 2.3. In red solid lines, we indicate the total flux, in blue dashed lines the contribution of the photo-pair production, in black dotted lines the flux due to charged pion production via photo-disintegration processes and to neutron disintegration, and in pale blue dash-dotted lines the contribution of the neutral pion channel.

cosmic-rays is fairly robust to changes in both composition and the configuration of magnetic fields. The normalization of the flux ultimately depends on the injected energy, namely, the cosmic-ray luminosity and the injection spectral index at the source. The cosmic-ray luminosity of the source may be inferred from the normalization to the measured flux of ultrahigh cosmic-rays once the source density is specified. The apparent density of ultrahigh energy cosmic-ray sources, which coincides with

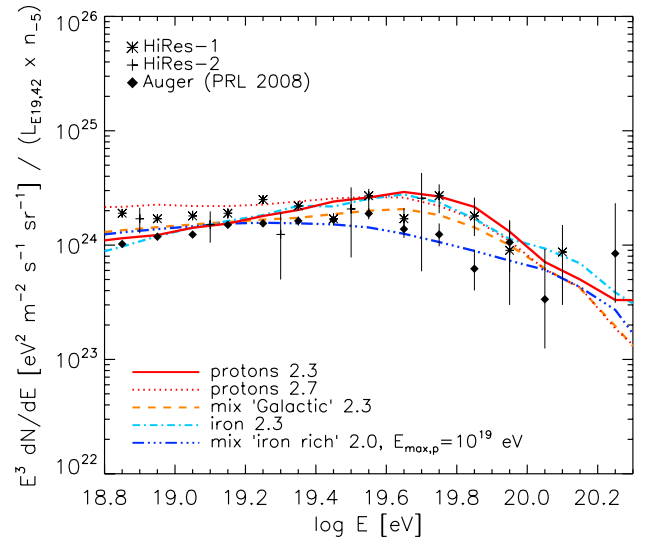


Fig. 5. Propagated spectra of ultrahigh energy cosmic-rays for various chemical compositions as described in Sect. 2.4 and the corresponding spectral indices that provide the best fit to the observational data. Sources are assumed to share an equal luminosity $L_{E,19} = 10^{42}$ erg s^{-1} and a spatial density $n_s = 10^{-5}$ Mpc^{-3} .

the true source density n_s for steady isotropic emitting sources (which we assume here; see Sect. 4 for a brief discussion of bursting/beamed sources), is bound by the lack of repeaters in the Pierre Auger dataset: $n_s \gtrsim 10^{-5}$ Mpc^{-3} (Kashti & Waxman 2008). This lower bound may in turn be translated into an upper limit to the gamma-ray flux expected from equal luminosity cosmic-ray sources, $L_{E,19} \lesssim 10^{42}$ erg/s.

Figure 5 presents the spectra obtained for sources of luminosity $L_{E,19} = 10^{42}$ erg s^{-1} and number density $n_s = 10^{-5}$ Mpc^{-3} . In each case, we represent the median spectrum of 1000 realizations of local source distributions, the minimum distance to a source being 4 Mpc. Our calculated values are comparable to the cosmic-ray fluxes detected by the two experiments HiRes and the Pierre Auger Observatory. The gamma-ray fluxes obtained for single sources with this normalization (i.e. a luminosity of $L_{E,19} = 10^{42}$ erg s^{-1}) at a distance of 100 Mpc are presented in Figs. 2–4.

These gamma-ray fluxes lie below the limits of detectability of current and upcoming instruments such as Fermi, HESS, and the Cherenkov Telescope Array (CTA), by more than two orders of magnitude. The sensitivity of the Fermi telescope is indeed of the order of $\sim 2 \times 10^{-10}$ $GeV s^{-1} cm^{-2}$ around 10 GeV for a year of observation and the future Cherenkov Telescope Array (CTA) is expected to have a sensitivity of order $\sim 10^{-11}$ $GeV s^{-1} cm^{-2}$ for 100 h, for a point source around TeV energies (Atwood et al. 2009; Wagner et al. 2009).

3.2. Rare and powerful sources

From the previous subsection, we conclude that only powerful sources embedded in magnetized environments, which are rare compared to the average population of ultrahigh energy cosmic-ray sources, may produce a gamma ray signature strong enough to be observed by current and upcoming experiments. In the following, we examine the case of two of these sources embedded in filaments, with (isotropic) luminosity chosen to

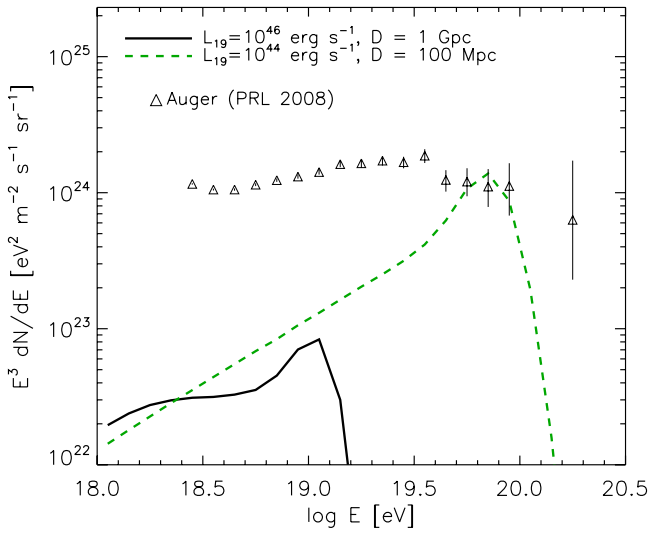


Fig. 6. Propagated spectra of ultrahigh energy cosmic-rays from a single source with luminosity $L_{E,19} = 10^{46} \text{ erg s}^{-1}$ located at a distance of $D = 1 \text{ Gpc}$ (black solid) or $L_{E,19} = 10^{44} \text{ erg s}^{-1}$ and $D = 100 \text{ Mpc}$ (green dashed). The injection spectral index is 2.0 in both cases. The observed Auger spectrum (Abraham et al. 2008b) is overlaid.

be higher than the average allowed by the cosmic-ray normalization for equal luminosity sources $L_{E,19} = 10^{44} \text{ erg s}^{-1}$ and $L_{E,19} = 10^{46} \text{ erg s}^{-1}$. As a case study, we place these sources at a distance of $D = 100 \text{ Mpc}$ and $D = 1 \text{ Gpc}$, respectively. These distances are consistent with the number density of objects found at comparable photon luminosities (see for example Wall et al. 2005).

The ultrahigh energy cosmic-ray spectra obtained after propagation from these two model sources are represented in Fig. 6. The injection at the source is assumed to consist purely of protons and have a spectral index of 2.0. The comparison with the Auger data shows that the close-by source (green dashed) is marginally excluded. More precisely, this source should produce a strong anisotropy signal, close to unity, relative to the all-sky background if the magnetic deflection at this energy $\sim 7 \times 10^{19} \text{ eV}$ is smaller than unity. Following Kotera & Lemoine (2008b), the expected deflection is about $2^\circ Z$ if one models the magnetized Universe as a collection of magnetized filaments with $B = 10 \text{ nG}$ ($\lambda_B = 100 \text{ kpc}$) immersed in unmagnetized voids of typical separation $\sim 40 \text{ Mpc}$. This estimate neglects the deflection due to the Galactic magnetic field, which depends on incoming direction and charge. Qualitatively speaking, however, one would then expect the above source to produce a strong anisotropy signal unless it injects only iron group nuclei with $Z \sim 26$ at the highest energies. In this latter case, however, the gamma-ray signal would be lower by a factor ~ 5 or even suppressed if $E_{\text{max,p}}$ were less than the pion production threshold, as discussed in the previous Section. Furthermore, this source might also induce a strong anisotropy at energies $\sim 3 \text{ EeV}$, depending on the ratio of the composition of injected protons to iron group nuclei (Lemoine & Waxman 2009).

In contrast, the remote source (indicated by the black solid line in Fig. 6) contributes to $\sim 10\%$ of the total flux around $E_{\text{cr}} \sim 10^{19} \text{ eV}$. This source would be completely invisible in ultrahigh energy cosmic-rays, because of the large expected magnetic deflection at this energy, on a large path length of 1 Gpc.

We now discuss the possibility of detecting these sources in gamma rays. Figure 7 presents our computed images of synchrotron gamma-ray emission for these two examples of sources embedded in the filament shown in Fig. 1.

However, one should be aware that the sensitivity of gamma-ray telescopes weakens for extended sources by the ratio of the radius of the emission to the angular resolution. Typically, Fermi LAT and HESS have an angular resolution of some fractions of a degree around energies of 10 GeV and 100 GeV, respectively. CTA has an even higher resolution of the order of the arc-minute above 100 GeV. For this reason, one will have to find a source with an acceptable range in luminosity and distance, so as not to lose too much flux due to the angular extension, but still being able to resolve this extension. We note that the magnetic configuration around the source should have a negligible role on the flux intensity, as we demonstrated in Sect. 2. However, the magnetic configuration, in particular the strength and the coherence length, directly controls the extension of the image, which is given by the transverse displacement of the protons by means of magnetic deflection (Gabici & Aharonian 2005).

Figure 8 demonstrates that the synchrotron gamma ray emission from both our model sources could be observed by Fermi LAT and CTA. Their flux integrated over the angular resolution of these instruments at $\sim 10 \text{ GeV}$ are indeed above their corresponding sensitivities. The case presented by a dashed green line is however marginally excluded by the observed spectrum of cosmic-rays and even more so by the search for anisotropy, as discussed previously (Fig. 6). It thus appears that the gamma-ray flux of a source of luminosity $L_{E,19} \sim 10^{44} \text{ erg s}^{-1}$ will be hardly observable, as placing the source at a greater distance to reconcile its spectrum with the observations will dilute the gamma-ray emission, below the current instrument sensitivities. The detection of extremely powerful sources with $L_{E,19} = 10^{46} \text{ erg s}^{-1}$ located around 1 Gpc is more promising. According to Fig. 8, the emission from these sources would spread over a fraction of a degree, hence their image could possibly be resolved by Fermi and certainly by CTA.

As discussed in the introduction, the observation of a multi-GeV extended emission as obtained in these images would provide clear evidence of acceleration to ultrahigh energies, provided that the possible background associated with a halo seeded by TeV photons can be removed. As discussed in Aharonian et al. (1994), Dai et al. (2002), d’Avezac et al. (2007), Elyiv et al. (2009), and Neronov & Semikoz (2009), the angular size of the latter signal is a rather strong function of the average intergalactic magnetic field. In particular, if the field is assumed to be homogeneous and of strength larger than 10^{-14} G , the image is diluted on large angular scales. Accounting for the inhomogeneity of the magnetic field (see Sect. 3.3 below for a detailed discussion), one concludes that the flux associated with this image, on a degree scale, is reduced by the filling factor of voids in which $B \lesssim 10^{-14} \text{ G}$ within $\sim 40 \text{ Mpc}$ of the source (this distance corresponding to the energy loss distance of the primary $\sim 20 \text{ TeV}$ photons). Furthermore, the angular size of the halo seeded by multi-TeV photons depends strongly on photon energy, i.e. $\delta\theta \propto E_\gamma^{-2}$ or $\delta\theta \propto E_\gamma^{-1.75}$ depending on λ_B (see Neronov & Semikoz 2009). In contrast, the synchrotron halo is more strongly peaked in energy around 10 GeV and in this range its angular size is essentially independent of energy, but is determined instead by the magnetic field strength and source distance. Assuming comparable total power in both signals, discrimination between them should thus be feasible, although all the more easier if the halo signal seeded by multi-TeV gamma-rays were diluted on large angular scales.

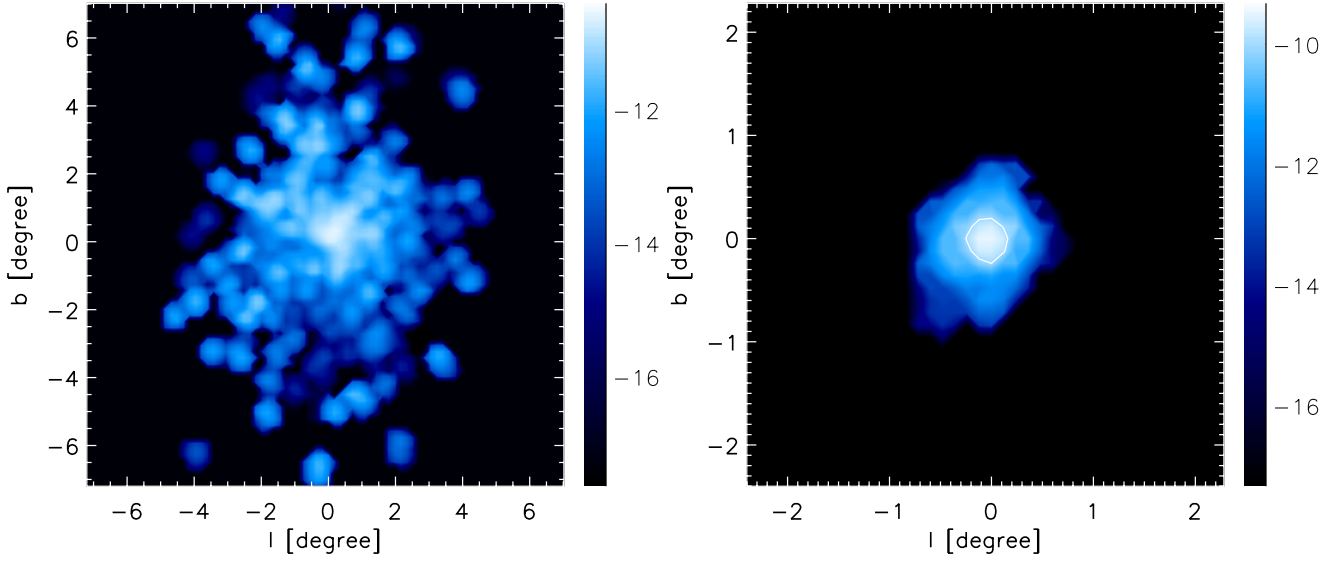


Fig. 7. Image of a filament in gamma-rays produced via synchrotron emission, integrated over $E_\gamma = 1\text{--}100$ GeV. We chose an “anisotropic” distribution of the magnetic field with normalization $B_0 = 1$ nG. *Left:* the filament is observed along its axis from a distance of 100 Mpc and the embedded source has a cosmic-ray luminosity of $L_{E,19} = 10^{44}$ erg s^{-1} . *Right:* the filament is observed along its axis from a distance of 1 Gpc and the embedded source has a luminosity of $L_{E,19} = 10^{46}$ erg s^{-1} . The color bar indicates the logarithm of the flux in $\text{GeV cm}^{-2} \text{s}^{-1}$. White contours indicate a flux level of 10^{-10} $\text{GeV cm}^{-2} \text{s}^{-1}$.

The previous discussion thus indicates that detection might be possible for powerful rare sources at distances in excess of 100 Mpc. However, one could not then argue, on the basis of the detection of a gamma-ray counterpart, that the source of ultrahigh energy cosmic-rays has been identified, as this source of gamma-rays must remain a rare event, which could not be considered a representative element of the source population of ultrahigh energy cosmic-rays. Overall, one finds that this source must contribute 10% of the flux at energies well below the GZK cut-off to be detectable in gamma-rays. We note that this conclusion does not depend on the degree of beaming of the emission of the source, as we discuss in Sect. 4.

To conclude this section an optimistic note, we discuss an effect that could improve the prospects for detection. In the above discussion and our simulations, following Gabici & Aharonian (2005), we have assumed that all the synchrotron emission takes place in the immediate environment of the source, because the magnetic field drops to low values outside the filament, where inverse Compton cascades would therefore become the dominant source of energy loss of the pairs. However, since the typical energy-loss length of ultrahigh energy cosmic-rays exceeds the typical distance between two filaments, one must in principle allow for the possibility that the beam of ultrahigh energy protons seeds secondary pairs in intervening magnetized filaments, which would then also contribute to the observed synchrotron emission. During the crossing of a filament, ultrahigh energy protons are deflected by an angle $\delta\theta_i \ll 1$ (unless the primary cosmic-ray carries a large charge or the filament is of unusual magnetisation, see the discussion in Kotera & Lemoine 2008b). Hence, as long as the small deflection limit applies, the problem is essentially one-dimensional and each filament contributes to the gamma-ray flux a fraction comparable to that of the source environment. The overall synchrotron signal would then be amplified by a factor λ/l_f , where λ denotes the relevant energy-loss length, $\lambda \sim 100$ Mpc for pion production of 10^{20} eV protons, $\lambda \sim 1$ Gpc for the pair production of 10^{19} eV protons and $l_f \sim 40$ Mpc is the typical separation between two filaments. Overall, one might expect an amplification as large as an order

of magnitude for the contribution to the flux by pair production, for sources located at several hundreds of Mpc, and a factor of a few for sources located at 100 Mpc and, correspondingly, an amplification factor $\sim 2\text{--}3$ for the contribution to the flux by pion production. Since the pair production channel contributes $\sim 10\%$ of the total flux at $E_\gamma \sim 10\text{--}100$ GeV for a pure proton composition, the amplification factor should remain limited to a factor of a few, unless the interaction length with magnetized regions is substantially smaller than the above (expected) $l_f = 40$ Mpc.

3.3. Inverse Compton cascades

We now briefly discuss the gamma-ray signal expected from Compton cascades of ultrahigh energy photons and pairs injected into the intergalactic medium. The physics of these cascades was discussed in detail in Wdowczyk et al. (1972), Protheroe (1986), Protheroe & Stanev (1993), Aharonian et al. (1994), Ferrigno et al. (2004), and Gabici & Aharonian (2007). The angular extent and time distribution of GeV–TeV gamma-rays resulting from inverse Compton cascades seeded by ultrahigh energy cosmic-rays produced by gamma-ray bursts was also discussed by Waxman & Coppi (1996). Inverse Compton cascades in the steady state regime were considered in the study of Armengaud et al. (2006, for a source located in a cluster of galaxies) but dismissed in the study of Gabici & Aharonian (2005) because of the dilution of the emitted flux through the large deflection of the pairs in the low energy range of the cascade. The effective inverse Compton cooling length of electrons of energy $E_e \lesssim 100$ TeV can indeed be written as $x_{e\gamma} \approx 3.5$ kpc $(E_e/100 \text{ TeV})^{-1}$ and on this distance scale, the deflection imparted by a magnetic field of coherence length $\lambda_B \gg x_{e\gamma}$ reads $\theta_e \sim x_{e\gamma}/r_{L,e} \sim 3 \times 10^{-2} (E_e/100 \text{ TeV})^{-2} (B/10^{-12} \text{ G})$. Then, assuming that the last pair of the cascade carries an energy $E_{\text{fin}} \sim 20$ TeV (so that the photon produced through the interaction with the CMB carries a typical energy $\lesssim 1$ TeV), one finds that a magnetic field larger than $\sim 10^{-12}$ G isotropizes the low energy cascade, in agreement with the estimates of Gabici & Aharonian (2005).

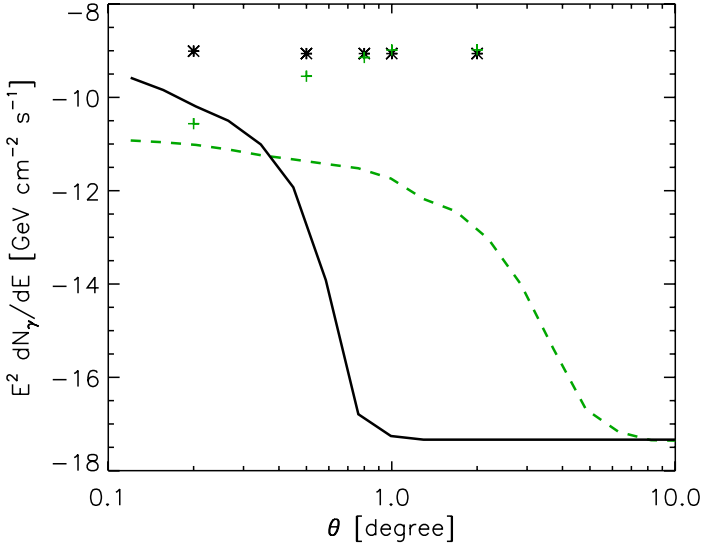


Fig. 8. Angular profiles of the images of the sources represented in Fig. 7. We represent the gamma-ray flux integrated over energies $E_\gamma = 1\text{--}100$ GeV averaged over angular bins, for a filament seen along its axis, at 1 Gpc and $L_{E,19} = 10^{46}$ erg s $^{-1}$ (black solid line), and at 100 Mpc and $L_{E,19} = 10^{44}$ erg s $^{-1}$ (green dashed line). The black stars and green crosses present the corresponding integrated flux up to a given angular extension in the sky θ .

This situation is modified when one takes into account the inhomogeneous distribution of extra-galactic magnetic fields, as we now discuss. Primary cosmic-rays, upon traveling through the voids of large-scale structure may inject secondary pairs, which undergo inverse Compton cascades in these unmagnetized regions. If the field in these regions is smaller than the above 10^{-12} G, then the cascade will transmit its energy in forward \lesssim TeV photons. Depending on the exact value of B where the cascade ends, the resulting image will of course be spread over some finite angle. Since we are interested in sharply peaked images, we consider a typical angular size θ and ignore these regions in which the magnetic field is large enough to contribute to the image on a size larger than θ . For $\theta \ll 1$, the problem remains one-dimensional as before, and one can compute the total energy injected in inverse Compton cascades within θ , as follows.

The luminosity injected in secondary pairs and photons up to distance d is written $\chi_e L_{\text{cr}}(>E)$. Since we are interested in the signatures of ultrahigh cosmic-ray sources, we require that $E \geq 10^{19}$ eV; for protons, the energy loss length due to pair production moreover increases dramatically as E becomes lower than 10^{19} eV, so that the contribution of lower energy particles can be neglected to a first approximation. For photo-pair production, the fraction transferred is $\chi_{e,ee} \approx d/1$ Gpc of $L_{E,19} = L_{\text{cr}}(>10^{19}$ eV) up to $d \sim 1$ Gpc. For pion production, the fraction of energy transferred is roughly $\chi_{e,\pi} \approx d/100$ Mpc of $L_{\text{cr}}(>6 \times 10^{19}$ eV) in the continuous energy loss approximation. At distances $100 \text{ Mpc} \leq d \leq 1 \text{ Gpc}$, the fraction χ_e of $L_{E,19}$ injected into secondary pairs and photons thus ranges from ~ 0.5 for $d = 100$ Mpc to ~ 1 at $d = 1$ Gpc; in short, it is expected to be of the order of unity or slightly less. All the energy injected in this way into sufficiently unmagnetized regions (see below) will be deposited through the inverse Compton cascade in the sub-TeV range, with a typical energy flux dependence $\propto E_\gamma^{1/2}$ up to some maximal energy $E_{\gamma,\text{max}} \sim 1\text{--}10$ TeV beyond which the Universe is opaque to gamma-rays on the distance scale d

(Ferrigno et al. 2004). Neglecting any redshift dependence for simplicity, the gamma-ray energy flux per unit energy interval may then be approximated as

$$\begin{aligned} E_\gamma^2 \frac{dN_\gamma}{dE_\gamma} &\approx f_{1d}(<B_\theta) \chi_e \frac{L_{\text{cr}}}{8\pi d^2} \left(\frac{E_\gamma}{E_{\gamma,\text{max}}} \right)^{1/2} \\ &\approx 2.5 \times 10^{-10} \text{ GeV cm}^{-2} \text{ s}^{-1} f_{1d}(<B_\theta) \chi_e \\ &\quad \times \frac{L_{E,19}}{10^{42} \text{ erg/s}} \left(\frac{d}{100 \text{ Mpc}} \right)^{-2} \left(\frac{E_\gamma}{E_{\gamma,\text{max}}} \right)^{1/2}, \end{aligned} \quad (6)$$

where $f_{1d}(<B_\theta)$ denotes the one-dimensional filling factor, i.e. the fraction of the line of sight in which the magnetic field is weaker than the value B_θ such that the deflection of the low energy cascade is θ . For reference, $B_\theta \sim 2 \times 10^{-14}$ G for $\theta \sim 1^\circ$. In general, one finds in the literature the three-dimensional filling factor f_{3d} , but $f_{1d}(<B_\theta) \sim f_{3d}(<B_\theta)$ up to a numerical prefactor of the order of unity that depends on the geometry of the structures. Interestingly enough, the amount of magnetization of the voids of large-scale structure is directly related to the origin of the large-scale magnetic fields. Obviously, if galactic and cluster magnetic fields originate from a seed field produced in a homogeneous way with a present-day strength $B \gg 10^{-14}$ G, then the above gamma-ray flux will be diluted on large angular scales, hence below the detection threshold. However, if the seed field, extrapolated to present-day values is much lower than this value, or if most of the magnetic enrichment of the intergalactic medium results from pollution by star-forming galaxies and radiogalaxies, then one should not expect $f_{1d}(<B_\theta)$ to be negligible. For instance, Donnert et al. (2009) obtain $f_{3d}(<10^{-14} \text{ G}) \sim \mathcal{O}(1)$ for these models. Given the sensitivity of current gamma-ray experiments such as HESS in the TeV energy range, the inverse Compton cascades might then produce degree-size detectable halos for source luminosities $\geq 10^{43} [f_{3d}(<10^{-14} \text{ G})]^{-1} (d/100 \text{ Mpc})^{-2}$ erg/s. For future instruments such as CTA, the detectability condition will be of the order of $L_s \geq 10^{41} [f_{3d}(<10^{-14} \text{ G})]^{-1} (d/100 \text{ Mpc})^{-2}$ erg/s. The expected flux level remains quite uncertain as it depends mostly on the configuration of the extragalactic magnetic field in the voids, in contrast to the synchrotron signal, which is controlled mainly by the source luminosity.

We note that intergalactic magnetic fields of strength $B \lesssim 10^{-15}$ G might be probed through the delay time of the high energy afterglow of gamma-ray bursts (Plaga 1995; Ichiki et al. 2008) or the GeV emission around blazars (Aharonian et al. 1994; Dai et al. 2002; d’Avezac et al. 2007; Murase et al. 2008; Elyiv et al. 2009; Neronov & Semikoz 2009), as discussed earlier. As the present paper was being refereed, some first estimates of the lower bounds to the average magnetic field appeared, giving $B \gtrsim 10^{-16}\text{--}10^{-15}$ G (see Neronov & Vovk 2010; Ando & Kusenko 2010; and Dolag et al. 2011).

3.4. Cen A

In view of the results of Sect. 3.1, one may also consider mildly powerful but nearby sources. One such potential source is Cen A, which has attracted a considerable amount of attention, as it is the nearest radiogalaxy (3.8 Mpc) and because a fraction of the Pierre Auger events above 60 EeV have been found to be clustered within $10\text{--}20^\circ$ of this source. As discussed in detail in Lemoine & Waxman (2009), this source is likely to be too weak to accelerate protons to $\geq 10^{19}$ eV in steady state, but heavy nuclei might possibly be accelerated to GZK energies. The acceleration of protons to ultrahigh energies in flaring episodes of

high luminosity was proposed in [Dermer et al. \(2009\)](#). We also recall that the apparent clustering in this direction can be naturally explained by a large concentration of matter in the local Universe, in the direction of Cen A but located further away. As discussed in [Lemoine & Waxman \(2009\)](#), some of the events detected toward Cen A could also be attributed to rare and powerful bursting sources located in the Cen A host galaxy, such as gamma-ray bursts. Owing to the scattering of the particles on the magnetized lobes, one would not be able to distinguish these bursting sources from a source located in the core of Cen A.

We have argued throughout this paper that a clear signature of ultrahigh energy cosmic-ray propagation could be produced in presence of an extended and strong magnetized region around the source. The magnetized lobes of Cen A provide such a site, with an extension of $R_{\text{lobe}} \sim 100$ kpc, a magnetic field of average intensity $B_{\text{lobe}} \sim 1 \mu\text{G}$, and a coherence length $\lambda_{\text{lobe}} \sim 20$ kpc ([Feain et al. 2009](#)). In terms of gamma-ray fluxes, one can calculate however that the only advantage of studying Cen A instead of the average types of sources described in Sect. 3.1 lies in its proximity. As noted before, the bulk of gamma-ray emission will be due to electrons and positrons produced by pion production with $E_e > 10^{19}$ eV. The flux of these secondary electron/positron emission scales as the distance r the primary protons travels through, as long as $r \ll \lambda$, where λ is the energy loss length by pion production. In our situation, to calculate the synchrotron gamma-ray flux, this distance corresponds to the size of the magnetized structure with $B \gtrsim 0.5$ nG ($E_e/10^{19}$ eV) $^{-3/4}$, namely $r \sim R_{\text{lobe}}$ in our toy-model. One may also note that considering the magnetic field strength in the lobes, the gamma-ray flux will peak around $E_{\gamma\text{syn}} \sim 6.8 \text{ TeV } B_{\text{lobe}} E_{e,19}^2$, according to Eq. (2). Scaling the expected flux from the lobes around 10 TeV $F_{\text{lobe},10 \text{ TeV}}$ to the flux that we calculated in Sect. 3.1 for standard sources embedded in filaments around 10 GeV $F_{\text{fil},10 \text{ GeV}}$, one obtains

$$F_{\text{lobe},10 \text{ TeV}} \sim \left(\frac{d_{\text{CenA}}}{d_{\text{fil}}} \right)^{-2} \frac{L_{\text{CenA}}}{10^{42} \text{ erg/s}} \frac{R_{\text{lobe}}}{5 \text{ Mpc}} F_{\text{fil},10 \text{ GeV}} \quad (7)$$

$$\sim 2 \times 10^{-14} \text{ GeV s}^{-1} \text{ cm}^{-2}, \quad (8)$$

which is far below current instrument sensitivities. Here, $d_{\text{CenA}} = 3.8$ Mpc and $d_{\text{fil}} = 100$ Mpc are the distance of Cen A and our model filament, respectively, and L_{CenA} is the cosmic-ray luminosity of Cen A, which we assume to be 10^{39} erg s $^{-1}$ according to constraints from ultrahigh energy cosmic-ray observations (see for example [Hardcastle et al. 2009](#)). Moreover, Cen A covers $\theta_{\text{source}} \sim 10^\circ$ in the sky, inducing a sensitivity loss of a factor $\theta_{\text{source}}/\theta_{\text{PSF}} \sim 10$ for the Fermi telescope (θ_{PSF} represents the angular resolution of the instrument).

All in all, taking into account all these disadvantages, we conclude that the synchrotron emission produced in the lobes of Cen A would be three orders of magnitudes weaker than the flux obtained for the average types of sources described in Sect. 3.1.

Our numerical estimate using the method introduced in Sect. 2.2 and modeling the lobes as spherical uniformly magnetized structures confirms this calculation. We note that the contribution of the pair production channel is not as suppressed as the other components. Owing to the strength of the magnetic field, the electrons and positrons radiating in synchrotron around 0.1–1 GeV are of lower energy than for the standard filament case ($E_e \sim 10$ MeV), thus more numerous. At these energies, the synchrotron emission in the filament are also partially suppressed by the shortening of the inverse Compton loss length as compared to the synchrotron loss length. Because of the high

magnetic field intensity, this effect is less pronounced in the lobe case.

Recently, Fermi LAT discovered gamma-ray emission emanating from the giant radio lobes of Cen A ([Cheung et al. 2010](#)). In light of our discussion, the ultrahigh energy cosmic-ray origin of this emission can be excluded. It could rather be interpreted as an inverse Compton scattered relic radiation on the CMB and infrared and optical photon backgrounds, as proposed by [Cheung et al. \(2010\)](#).

In addition, we note that [Kachelrieß et al. \(2009\)](#) estimated the gamma-ray fluxes emitted as a result of the production of ultrahigh energy cosmic-rays in Cen A. These authors conclude that a substantial signal could be produced, well within the detection capabilities of Fermi and CTA. However, this signal results from interactions of cosmic rays accelerated inside the source, not outside. As we discussed before, this gamma-ray signal, i.e., one that could not be angularly resolved from the source, could not be interpreted without ambiguity. In particular, one would not be able to discriminate it from a secondary signal produced by multi-TeV leptons or hadrons accelerated in the same source. Furthermore, the gamma-ray signal discussed in [Kachelrieß et al. \(2009\)](#) is mainly attributed to cosmic-rays at energies $\lesssim 10^{18}$ eV, not to ultrahigh cosmic-rays above the ankle, although the generation spectrum in the source is normalized to the Pierre Auger Observatory events at $\gtrsim 6 \times 10^{19}$ eV. The conclusions thus depend rather strongly on the shape of the injection spectrum as well as on the phenomenological modelling of acceleration, as clearly shown by Fig. 1 of their study.

Finally one may turn to the highest energies and search for ultrahigh energy cosmic-ray signatures from Cen A by looking directly at the ultrahigh energy secondary photons produced during the propagation. These photons should indeed not experience cascading at this close distance. [Taylor et al. \(2009\)](#) studied this potential signature and concluded that Auger should be able to detect 0.05–0.075 photon per year from Cen A, assuming that it is responsible for 10% of the $>6 \times 10^{19}$ eV cosmic-ray flux, and assuming a 25% efficiency for photon discrimination.

4. Discussion and conclusions

We first recap our main findings. We have discussed the detectability of gamma-ray halos of ultrahigh energy cosmic-ray sources, relaxing most of the assumptions made in previous studies. We have focused our study on the synchrotron signal emitted by secondary pairs, which offers a possibility of unambiguous detection. In this study, we have taken into account the inhomogeneous distribution of the magnetic field in the source environment and examined the effects of non pure proton composition on the gamma-ray signal. We have found that the gamma-ray flux predictions are rather robust with respect to the uncertainties attached to these physical parameters. The normalization and hence the detectability of this flux ultimately depends on the energy injected into the primary cosmic-rays, for realistic values of the magnetic field. We have further demonstrated that the average type of sources contributing to the ultrahigh energy cosmic-ray spectrum produces a gamma-ray flux more than two orders of magnitudes lower than the sensitivity of the current and upcoming instruments. Rare powerful sources contributing more than 10% to the cosmic-ray flux would be more promising targets in terms of detectability. We have found that the gamma-ray signatures of these sources could be detectable provided that they are located far enough not to overshoot the observed cosmic-ray spectrum. If the extended emission of such signatures were resolved (which should be the case with Fermi

and CTA), such a detection would provide an evidence of the acceleration of cosmic-rays to energies $\gtrsim 10^{19}$ eV. However, as we have discussed, these gamma-ray sources are probably exceptional and could not be considered as representatives of the population of ultrahigh energy cosmic-ray sources. We have also discussed the deflection and the dilution of the Compton cascading gamma-ray signal at sub-TeV energies. In this case, the flux prediction depends sensitively on the filling factor of the magnetic field with values smaller than $\sim 10^{-14}$ G in the voids of large-scale structure. If this latter value is larger than a few percent, as suggested by some scenarios for the origin of cosmic magnetic fields, then the inverse Compton cascade could provide a degree-size image of the ultrahigh cosmic-ray source, with a flux slightly higher than that associated with the synchrotron component.

Finally, we have also discussed the detection of nearby sources, considering the radiogalaxy Centaurus A as a prototypical example. We have demonstrated that, *if* ultrahigh energy cosmic-rays were produced in Cen A, their secondary gamma-ray halo signature should not be detectable by current experiments. Our conclusion indicates in particular that the gamma-ray emission detected by Fermi LAT from the giant radio lobes of Cen A (Cheung et al. 2010) cannot result from the synchrotron radiation of ultrahigh energy secondaries in that source.

We need to stress that, in our discussion, we have systematically assumed that the source emits cosmic-rays at a steady rate isotropically. We briefly discuss these assumptions. If the source is instead of the flaring type, then, at a similar cosmic-ray source luminosity, the flux predictions will be reduced by the ratio of the source flare duration Δt to the dispersion in arrival times σ_t that results from propagation in intergalactic magnetic fields. In theoretical models, Δt can take values ranging from a few seconds for gamma-ray bursts (Milgrom & Usov 1996; Waxman 1995; Vietri 1995) to days in the case of blazar flares, while σ_t is typically expected to be of the order of 10^3 – 10^5 yrs for protons of energy $\gtrsim 70$ EeV (see Kotera & Lemoine 2008b, for a detailed discussion). In both cases, the high luminosity injected during the flaring episodes is insufficient to compensate for the dilution in arrival times. Of course, if the source is a repeater, with a timescale between two flaring episodes shorter than the intergalactic dispersion timescale, then one recovers a steady emitting situation, its effective luminosity being reduced by the fraction of time during which the source is active.

This latter situation may well apply to powerful radiogalaxies that produce ultrahigh energy cosmic-rays with flaring activity, since the size and magnetization of the jets and lobes are sufficient to deflect ultrahigh energy cosmic-rays by an angle of the order of unity, thereby dispersing them in time over $\sim R_{\text{lobe}}/c \sim 3 \times 10^5$ yr, with $R_{\text{lobe}} \sim 100$ kpc the typical transverse scale of the lobes. Even if ultrahigh energy cosmic-rays are ejected as neutrons, as discussed for instance by Dermer et al. (2009), a substantial fraction of these cosmic-rays will suffer dispersion as the decay length of neutrons of energy E_n is $0.9(E_n/10^{20} \text{ eV}) \text{ Mpc}$. In such a configuration, the source would effectively emit its cosmic-rays isotropically, as we have assumed.

Nonetheless, we consider beamed sources, for the sake of completeness. If one considers a single source, emitting cosmic rays in a solid angle $\Delta\Omega_s < 4\pi$, then at a similar total luminosity as an isotropic source, the luminosity emitted per steradian is larger by $4\pi/\Delta\Omega_s$ and so is the expected gamma-ray flux (in the limit of small deflection around the source, which is necessary for detection). In other words, the required total cosmic-ray luminosity per source for detection of gamma-rays is lowered by a

factor $\Delta\Omega_s/(4\pi)$. However, at a fixed contribution of the source to the cosmic-ray flux, the expected gamma-ray flux does not depend on the beaming angle. This is because both the cosmic-ray flux and the gamma-ray flux are determined by the produce of the number of visible sources and the luminosity per steradian². In particular, our conclusion that a source must contribute more than 10% to the ultrahigh energy cosmic-ray flux in order for the synchrotron signal to be detectable remains unchanged if $\Delta\Omega_s < 4\pi$.

Acknowledgements. We thank Eric Armengaud, Stefano Gabici, Susumu Inoue, Simon Prunet, and Michael Punch for helpful discussions. We thank Christophe Pichon for helping us identify adequate filaments in our cosmological simulation cube using his skeleton program, and Stéphane Colombi for providing us with the dark matter cosmological simulation cube. K.K. is supported by the NSF grant PHY-0758017 and by Kavli Institute for Cosmological Physics at the University of Chicago through grant NSF PHY-0551142 and an endowment from the Kavli Foundation.

References

- Abbasi, R. U., Abu-Zayyad, T., Archbold, G., et al. 2005, *ApJ*, 622, 910
 Abbasi, R. U., Abu-Zayyad, T., Al-Seady, M., et al. 2010, *Phys. Rev. Lett.*, 104, 161101
 Abraham, J., Abreu, P., Aglietta, M., et al. 2007, *Science*, 318, 938
 Abraham, J., Abreu, P., Aglietta, M., et al. 2008a, *Astropart. Phys.*, 29, 188
 Abraham, J., Abreu, P., Aglietta, M., et al. 2008b, *Phys. Rev. Lett.*, 101, 061101
 Abraham, J., P. Abreu, M. Aglietta, et al. 2009 [arXiv:0906.2319]
 Abraham, J., Abreu, P., Aglietta, M., et al. 2010, *Phys. Rev. Lett.*, 104, 091101
 Aharonian, F. A. 2002, *MNRAS*, 332, 215
 Aharonian, F. A., Coppi, P. S., & Voelk, H. J. 1994, *ApJ*, 423, L5
 Aharonian, F. A., Kelner, S. R., & Grigorieva, A. Y. 2010, *Phys. Rev. D*, 82, 043002
 Allard, D., Ave, M., Busca, N., et al. 2006, *J. Cosmology Astro-Particle Phys.*, 9, 5
 Allard, D., Busca, N. G., Decerprit, G., Olinto, A. V., & Parizot, E. 2008, *J. Cosmology Astro-Particle Physics*, 10, 33
 Ando, S., & Kusenko, A. 2010, *ApJ*, 722, L39
 Armengaud, E., Sigl, G., & Miniati, F. 2006, *Phys. Rev. D*, 73, 083008
 Atwood, W. B., Abdo, A. A., Ackermann, M., et al. 2009, *ApJ*, 697, 1071
 Berezhinsky, V., Gazizov, A., & Grigorieva, S. 2006, *Phys. Rev. D*, 74, 043005
 Bird, D. J., Corbatò, S. C., Dai, H. Y., et al. 1993, *Phys. Rev. Lett.*, 71, 3401
 Casse, F., Lemoine, M., & Pelletier, G. 2002, *Phys. Rev. D*, 65, 023002
 Cheung, C. C., Fukazawa, Y., Knödlseder, J., Stawarz, L., & Fermi-LAT collaboration. 2010, *BAAS*, 41, 440
 Clark, T. A., Brown, L. W., & Alexander, J. K. 1970, *Nature*, 228, 847
 Dai, Z. G., Zhang, B., Gou, L. J., Mészáros, P., & Waxman, E. 2002, *ApJ*, 580, L7
 Das, S., Kang, H., Ryu, D., & Cho, J. 2008, *ApJ*, 682, 29
 d’Avezac, P., Dubus, G., & Giebels, B. 2007, *A&A*, 469, 857
 Dermer, C. D., Razzaque, S., Finke, J. D., & Atayan, A. 2009, *New J. Phys.*, 11, 065016
 Dolag, K. 2006, *Astron. Nachr.*, 327, 575
 Dolag, K., Grasso, D., Springel, V., & Tkachev, I. 2004, *J. Korean Astron. Soc.*, 37, 427
 Dolag, K., Grasso, D., Springel, V., & Tkachev, I. 2005, *J. Cosmology Astro-Particle Physics*, 1, 9
 Dolag, K., Kachelriess, M., Ostapchenko, S., & Tomas, R. 2011, *ApJ*, 727, L4
 Donnert, J., Dolag, K., Lesch, H., & Müller, E. 2009, *MNRAS*, 392, 1008
 Elyiv, A., Neronov, A., & Semikoz, D. V. 2009, *Phys. Rev. D*, 80, 023010
 Feain, I. J., Ekers, R. D., Murphy, T., et al. 2009, *ApJ*, 707, 114
 Ferrigno, C., Blasi, P., & de Marco, D. 2004, *Nuclear Physics B Proceedings Supplements*, 136, 191
 Gabici, S., & Aharonian, F. A. 2005, *Phys. Rev. Lett.*, 95, 251102
 Gabici, S., & Aharonian, F. A. 2007, *Ap&SS*, 309, 465
 Gould, R. J., & Rephaeli, Y. 1978, *ApJ*, 225, 318
 Gould, R. J., & Schröder, G. P. 1967, *Phys. Rev.*, 155, 1408
 Hardcastle, M. J., Cheung, C. C., Feain, I. J., & Stawarz, L. 2009, *MNRAS*, 393, 1041
 Ichiki, K., Inoue, S., & Takahashi, K. 2008, *ApJ*, 682, 127

² The amount of magnetic deflection suffered during propagation in extra-galactic magnetic fields does not affect this result, as the larger number of visible sources for a larger amount of deflection is compensated by the dilution of the flux of each source.

- Kachelrieß, M., Ostapchenko, S., & Tomàs, R. 2009, *New J. Phys.*, 11, 065017
- Kashti, T., & Waxman, E. 2008, *J. Cosmology Astro-Particle Physics*, 5, 6
- Kelner, S. R., & Aharonian, F. A. 2008, *Phys. Rev. D*, 78, 034013
- King, E. J., & Coles, P. 2006, *MNRAS*, 365, 1288
- Kotera, K., Allard, D., Murase, K., et al. 2009, *ApJ*, 707, 370
- Kotera, K., & Lemoine, M. 2008a, *Phys. Rev. D*, 77, 023005
- Kotera, K., & Lemoine, M. 2008b, *Phys. Rev. D*, 77, 123003
- Lee, S. 1998, *Phys. Rev. D*, 58, 043004
- Lemoine, M., & Waxman, E. 2009, *JCAP*, 0911, 009
- Milgrom, M., & Usov, V. 1996, *Astropart. Phys.*, 4, 365
- Mücke, A., Rachen, J. P., Engel, R., Protheroe, R. J., & Stanev, T. 1999, *Publications of the Astronomical Society of Australia*, 16, 160
- Murase, K., Takahashi, K., Inoue, S., Ichiki, K., & Nagataki, S. 2008, *ApJ*, 686, L67
- Neronov, A., & Semikoz, D. V. 2009, *Phys. Rev. D*, 80, 123012
- Neronov, A., & Vovk, I. 2010, *Science*, 328, 73
- Plaga, R. 1995, *Nature*, 374, 430
- Protheroe, R. J. 1986, *MNRAS*, 221, 769
- Protheroe, R. J., & Stanev, T. 1993, *MNRAS*, 264, 191
- Ryu, D., Kang, H., & Biermann, P. L. 1998, *A&A*, 335, 19
- Sigl, G., Miniati, F., & Enßlin, T. A. 2004, *Phys. Rev. D*, 70, 043007
- Stecker, F. W. 1973, *Ap&SS*, 20, 47
- Stecker, F. W., Malkan, M. A., & Scully, S. T. 2006, *ApJ*, 648, 774
- Taylor, A. M., Hinton, J. A., Blasi, P., & Ave, M. 2009, *Phys. Rev. Lett.*, 103, 051102
- Unger, M., Engel, R., Schüssler, F., Ulrich, R., & Pierre AUGER Collaboration. 2007, *Astron. Nachr.*, 328, 614
- Vietri, M. 1995, *ApJ*, 453, 883
- Wagner, R. M., Lindfors, E. J., Sillanpää, A., et al. 2009, [[arXiv:0912.3742](https://arxiv.org/abs/0912.3742)]
- Wall, J. V., Jackson, C. A., Shaver, P. A., Hook, I. M., & Kellermann, K. I. 2005, *A&A*, 434, 133
- Waxman, E. 1995, *Phys. Rev. Lett.*, 75, 386
- Waxman, E., & Bahcall, J. N. 1999, *Phys. Rev. D*, 59, 023002
- Waxman, E., & Coppi, P. 1996, *ApJ*, 464, L75
- Wdowczyk, J., Tkaczyk, W., & Wolfendale, A. W. 1972, *J. Phys. A Math. Gen.*, 5, 1419